International Journal of Heat and Mass Transfer 112 (2017) 814–824

Contents lists available at ScienceDirect

International Journal of Heat and Mass Transfer

journal homepage: www.elsevier.com/locate/ijhmt

Experimental investigation on convective heat transfer of supercritical RP-3 in vertical miniature tubes with various diameters

Yanchen Fu, Haoran Huang, Jie Wen *, Guoqiang Xu, Wei Zhao

National Key Laboratory of Science and Technology on Aero-Engine Aero-Thermodynamics, Collaborative Innovation Center of Advanced Aero-Engine, School of Energy and Power Engineering, Beihang University, Beijing 100191, China

ARTICLE INFO

Article history:
Received 16 January 2017
Received in revised form 19 March 2017
Accepted 3 May 2017
Available online 15 May 2017

Keywords:
Convective heat transfer
Buoyancy
Vertical tube
Supercritical pressure
Various diameters

ABSTRACT

This article presents convective heat transfer of hydrocarbon fuel RP-3 at supercritical pressures in vertical micro-tubes with inner diameters of 0.538 mm, 1.09 mm and 1.82 mm under heating conditions. Effects of system pressure, heat flux, mass flow rate and flow direction were experimented and analyzed with wide range of supercritical status. Also, inner diameter effect on heat transfer were compared at identical conditions. The results indicate that sharp variation of thermal properties with temperature is the key factor to influence heat transfer. Normal, deterioration and enhancement heat transfer phenomena generally occur in turn along with dimensionless position. Moreover, Nusselt number variation shows good agreement when the contrast temperature T_b/T_{pc} is lower than 0.80 and $Bo^* = 1.0 \times 10^{-8}$ could be the critical point to evaluate buoyancy influence. At last, two well-predicted empirical correlations of Nusselt number are proposed for downward and upward flow heat transfer in 1.09 mm tube.

1. Introduction

Flow and heat transfer researches on supercritical fluid have been the key point in the area of energy since 1960s. Based on the background of supercritical pressure boiler and water cooled reactor, researchers all over the world widely studied flow and heat transfer characteristics at supercritical pressures for many pure liquids, such as water, carbon dioxide, and R122. Bourke et al. [1] experimentally investigated convective heat transfer of supercritical CO_2 in a stainless steel tube with 22.8 inner diameter. The results show that local heat transfer deterioration happens at the upstream part of experimental tube due to the inhibition of turbulent kinetic energy. In addition, the degree of heat transfer deterioration reduces gradually along with the increase of mass flow rate. Yamagata et al. [2] studied heat transfer characteristics of water at pressure of 22.6–29.4 MPa flowing in vertical and horizontal tubes. The heat flux varies from 116 kW/m^2 to 930 kW/m^2. It is indicated that heat transfer coefficient near pseudo-critical point increases at the low heat flux conditions and decreases at large heat flux conditions. The relative value between heat flux and mass flow rate (q/G) has huge influence on heat transfer, which is also concluded in Krasnoshchekov research [3]. Moreover, inner wall temperature would be sharply going up at the pseudo critical point at the condition of low mass flow rate and high heat flux. Jackson and Hall [4,5] systematically analyzed mechanisms of heat transfer enhancement and deterioration in different flow directions. It is demonstrated that buoyancy could change the distribution of fluid shear force near the wall and then induce the variation of turbulent kinetic energy. Thus, the heat transfer and flow resistance would change at some location positions. In the subsequent studies [6,7], dimensionless criterions such as $Gr_b/Re_b^{2.7}$ were proposed to judge buoyancy effect. Also, the results reveal that heat transfer is enhanced in the downward flow and similar phenomena are observed in other researches [8–10]. Jiang and his group [11–14] used experimental and numerical methods to study heat transfer characteristics of supercritical CO_2 in small tubes with various diameters. The results show that buoyancy leads to the local heat transfer deterioration at large heat flux and the wall temperature shows a trend of non-linear variation, even when the inlet Reynolds number is about 9000. Yamashita et al. [15] investigated flow resistance characteristics of supercritical HCFC22 in a vertical tube with diameter 4.4 mm. Significant increase is observed near the pseudo-critical point and the increase level decreases with the increase of heat flux.

With the developing emphasis of CCA (cooled cooling air) technology [16,17] in aero-engine, flow and heat transfer characteristics are widely studied as hydrocarbon fuel is used as a typical coolant. Hydrocarbon fuel is at the status of supercritical pressure since the fuel pumping pressure is about 3.45–6.89 MPa in typical

* Corresponding author.
E-mail address: wenjie@buaa.edu.cn (J. Wen).

http://dx.doi.org/10.1016/j.ijheatmasstransfer.2017.05.008
0017-9310/

Nomenclature

A	surface area
$Bo*$	buoyancy number
C_p	isobaric specific heat capacity (kJ/kg K)
d	diameter (m)
D	helical diameter (m)
g	gravitational acceleration (m/s^2)
G	mass flow rate (kg/(m^2 s))
Gr	Grashof number
H	enthalpy (kJ/kg)
h	heat transfer coefficient (W/(m^2 K))
I	electrical current (A)
Kv	thermal acceleration number
k	thermal conductivity (W/(m K))
L	length (m)
m	mass flux (g/s)
Nu	Nusselt number
P	pressure (MPa)
Pr	Prandtl number
Q	heat (W)
q	heat flux (kW/m^2)
$R(T)$	electronic resistivity (Ω m)
r	radius (m)
T	temperature (K)
Re	Reynolds number
U	voltage (V)

Greek

Φ	heat power (W)
ε	uncertainty
ρ	density (kg/m^3)
η	dynamic viscosity (Pa s)
β	isothermal compression coefficient (1/Pa)
ν	kinetic viscosity (m^2/s)
λ	thermal conductivity (W/(m K))

Subscripts

b	bulk
c	critical
f	film
in	inside
out	outside
pc	pseudo-critical
w	wall
x	local position

aero-engines. Brad Hitch and Karpuk [18,19] took experimental studies on heat transfer and thermal stability characteristics of hydrocarbon fuel JP-7 and MCH at supercritical pressures. Significant mass flow rate, pressure and temperature oscillations are observed during the experiments when the relative pressure (P/P_c) is below 1.5 and inner wall temperatures are higher than pseudo-critical temperatures. Furthermore, forced and natural convections are induced mixing to generate the sharp decrease of heat transfer coefficient and increase of wall temperature while the relative pressure is >2. Hines [20] conducted experiments to investigate heat transfer of hydrocarbon fuel RP-2 at various pressures. It is indicated that system pressure has oscillation frequency in the range of 100 Hz–15 kHz with 13.1 bar amplitude at the section of pseudo-critical temperature. Heat transfer coefficient of fuel side could be enhanced by 40% due to oscillations. Over recent years, many researchers [21–28] in China have devoted investigations on flow and heat transfer of pure hydrocarbon fuel and aviation kerosene RP-3, and obtained some meaningful conclusions. Zhang et al. [29] studied heat transfer characteristics of RP-3 flowing in vertically downward miniature tube with 1.8 mm inner diameter. It is noted that heat transfer deterioration happened at the condition of buoyancy factor $Bo^* < 1.6 \times 10^{-10}$ or thermal acceleration parameter $Kv < 1.5 \times 10^{-8}$. Sun et al. [30] compared experimental and numerical results of supercritical RP-3 at 5 MPa pressure in a horizontal circular tube. It is found that the modified k-ε model with correction of decreasing $C_{\varepsilon 1}$ and increasing $C_{\varepsilon 2}$ is more suitable than the standard k-ε model. In addition, discrepancy between calculated and experimental Nusselt number is limited within 10% relative error range.

Above all the research about supercritical fluid heat transfer, most of experimental and numerical models are conducted only in one diameter circular tube. Yildiz and Groeneveld [31] gave a brief review of diameter effect on supercritical heat transfer. Some typical research data like Ackerman [32], Song et al. [33], Kim et al. [9] and others [34–36] are summarized in tubes with a diameter range from 3.18 mm to 38.1 mm. The fluids are carbon dioxide, water, R-22, R-12 and it is summarized that heat transfer coefficient appears to decrease with an increase in tube diameter in the deteriorated heat transfer model. Considering the real application of heat exchanger with light-weight and compactness in aero-engine, tube with small diameter is essential to be the unit of heat exchange equipment. Thus, this paper experimentally investigated heat transfer characteristics of Chinese aviation kerosene RP-3 flowing in vertical small tubes with various diameters.

2. Experimental

2.1. System description

The whole experiments were conducted in the system of flow and heat transfer on supercritical fluid in Beihang University as shown in Fig. 1. The hydrocarbon fuel was pumped by an infusion pump (SP6015, 15 MPa; 0.01–600 ml/min) from the fuel tank. The pump could serve fixed mass flow rate controlled by the screen panel and keep the system pressure stable. Before the fuel flowed into the pump, one filter was set to obtain liquid without impurities. Then, the fuel mass flow rate was measured using a Coriolis-force flow meter (Model: DMF-1-1, 0.15%, Sincerity). The bypass fuel path was set at the pump outlet and one back pressure valve was used to adjust the system pressure up to 15 MPa. There were two preheated sections connected before the test section in order to guarantee the experimental inlet temperature in the wide range. Each preheated section was controlled independently by DC power with capacity of 20 kW.

Two K-type armored thermocouples with wire diameter of 0.5 mm were inserted through joints to measure inlet and outlet fuel temperatures. The system static pressure was measured by a pressure gage transducer (Model 3051CA4, Rosemount) at the outlet of test section. After flowing through the test section, the hot fuel was cooled down to room temperature by fuel-water cooler and then collected to the waste fuel barrels. The measured experimental data includes static pressure, temperature, mass flow rate, heating voltage and current, and these were exported in the form of electrical signals. All signals were gathered by ADAM-4018 data acquisition, transformed by ADAM-4520 to several documents and stored in the computer.

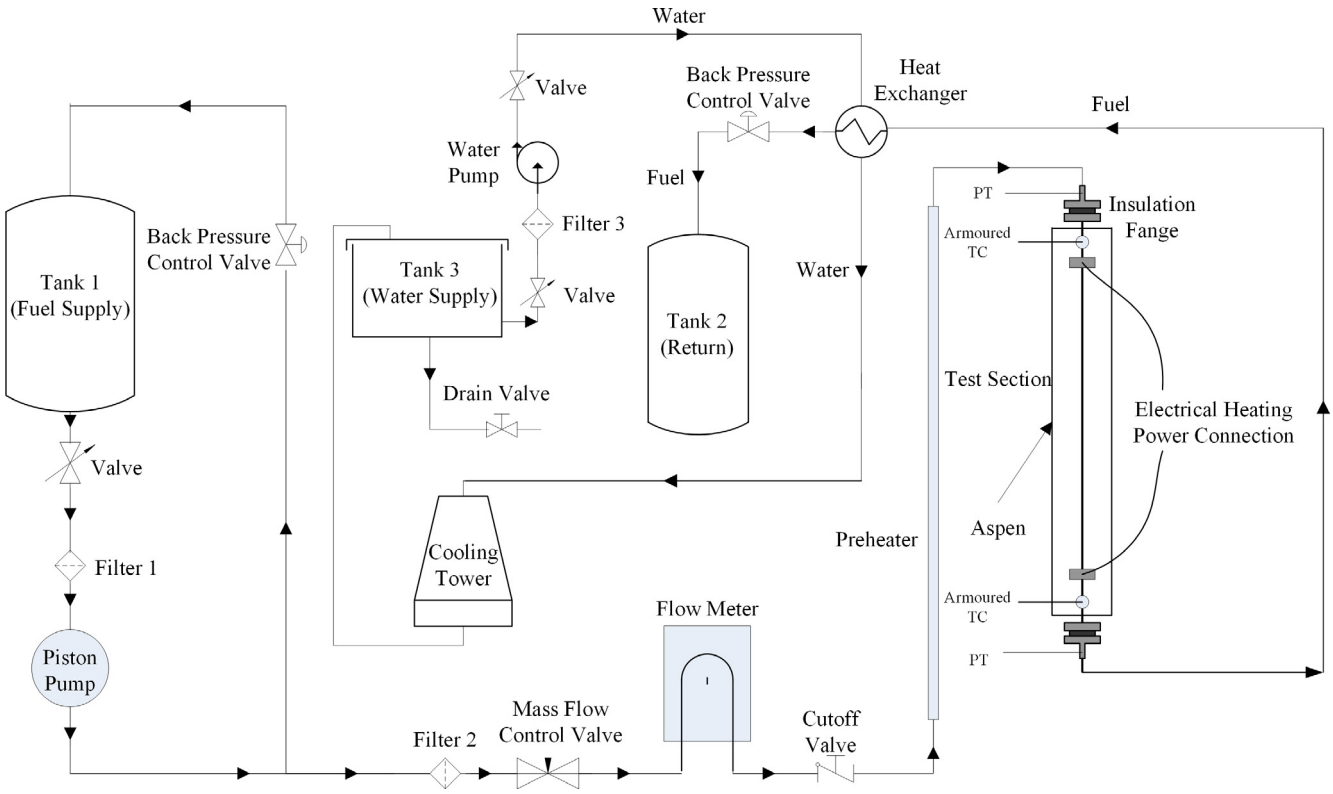

Fig. 1. Schematic of experimental system.

2.2. Test tubes

The experimental section is stainless steel (1Cr18Ni9Ti) straight tubes with three different inner diameters: 0.538 mm, 1.09 mm and 1.82 mm. Before the experiments, inner diameters of three different tubes were measured by scanning electron microscope (SEM, Scam3200, and Oxford, UK) and all the accurate inner diameters were confirmed as given in Fig. 2. Tube with 1.09 mm inner diameter was set as the standard tube to investigate. Fig. 3 shows that the whole tube length is 1000 mm with 800 mm heating section and 100 mm adiabatic inlet section is used to guarantee the flow fully developed. 20 thermocouples were uniformly welded onto the outer side of the tube wall to monitor wall temperatures. Pressure-fit connector was attached to experimental tube by silver welding to reduce the local flow resistance. The whole heating straight tube is covered by an insulation material called Aspen to reduce the heat loss. Many physical factors influences on heat transfer were considered and the detailed working conditions are shown in Table 1.

2.3. Data process

To calculate the local heat transfer coefficient along the test tube, the following equation is used.

$$h_x = \frac{q_x}{T_{wx,in} - T_{bx}} \tag{1}$$

As outer wall temperature is measured, the inner wall temperature could be calculated by one-dimensional pipeline heat transfer formula with internal heat source.

$$\frac{1}{r}\frac{\partial}{\partial r}\left(\lambda r \frac{\partial T}{\partial r}\right) + \dot{\Phi} = 0 \tag{2}$$

In which $\dot{\Phi} = \frac{I^2 R(T)}{\pi^2 (r_{out}^2 - r_{in}^2)^2}$, and the boundary condition is defined

$$r = r_{out}, \quad \lambda \frac{\partial T}{\partial r} = q_{\text{loss}}(i) \text{ and } T = T_{wo} \tag{3}$$

Thus, the inner wall temperature is obtained by definite integral from r_{in} to r_{out}.

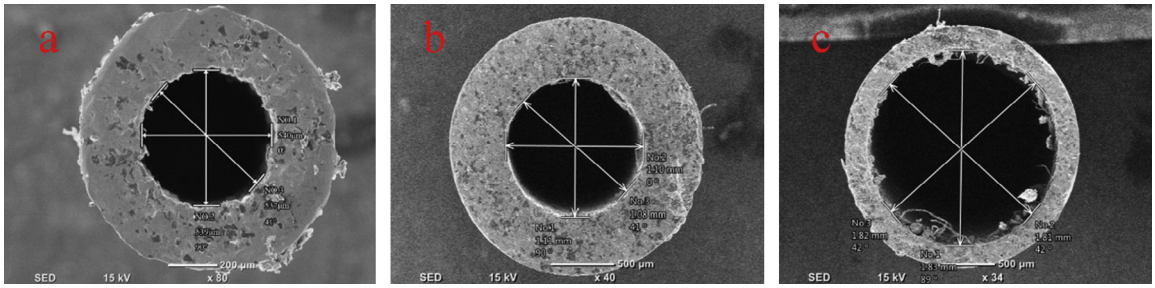

Fig. 2. Tube inner diameter photograph by SEM (a: 0.538 mm, b: 1.09 mm, c: 1.82 mm).

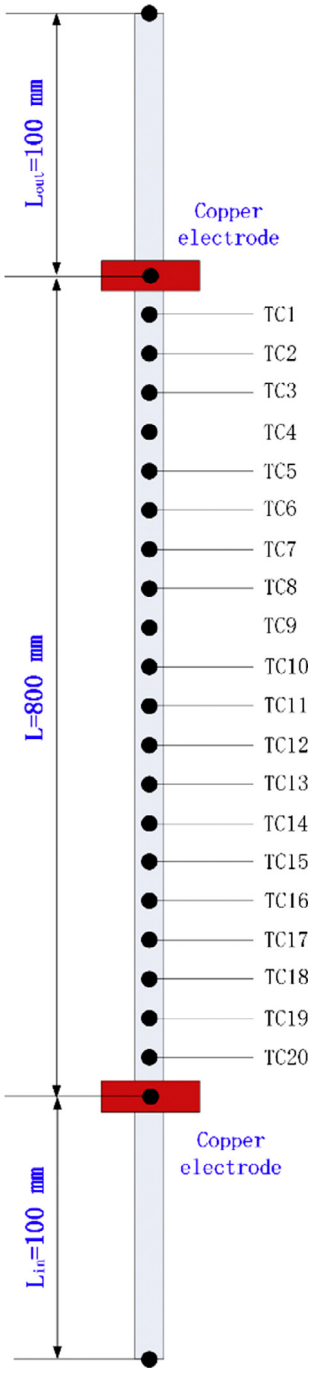

Fig. 3. Thermocouples distribution schematic of test section.

Table 1
Experimental parameters.

Parameter	Range
System pressure (MPa)	3,4,5
Mass flow rate (g/s)	1.0–2.0
Heat flux (kW/m^2)	90.5–600
Inlet temperature (K)	373–523
Flow direction	Upward, downward

$$T_{wx,in} = T_{wx,out} - \left[\left(\dot{\Phi}\frac{r_{out}^2}{2} - q_{x,loss}r_{out}\right)\ln\frac{r_{out}}{r_{in}} - \frac{\dot{\Phi}}{4}\left(r_{out}^2 - r_{in}^2\right)\right] \Big/ k_x \tag{4}$$

k_x is stainless steel local thermal conductivity. $q_{loss,x}$ is local heat loss and its value was measured and fitted by the relationship with temperature difference between ambient and tube wall. Furthermore, the effective heat flux q_x is defined as follows

$$q_x = \frac{I^2R(T)/[\pi\left(d_{out}^2 - d_{in}^2\right)/4]}{\pi d} - q_{loss,x} \tag{5}$$

The local fuel bulk temperature in the micro-tube can be calculated according to the wall heating power and the experimental RP-3 enthalpy-difference curve [37].

$$T_b(x) = H^{-1}\left[\frac{Q_x}{\dot{m}} + H(T_{in})\right] \tag{6}$$

In which $Q_x = I^2\int_0^x\left(R(T)\frac{x}{A}\right)dx - \pi d_{out}\int_0^x q_{loss}dx$ is the heating power from the inlet to the position x. At last, the local Nusselt number is defined in the following equation.

$$Nu_x = \frac{h_x d}{\lambda_x} \tag{7}$$

where λ_x represents local thermal conductivity of hydrocarbon fuel RP-3.

2.4. Uncertainty analysis

Since 1.09 mm inner diameter tube is chosen as the standard test tube, the following analysis is limited within 1.09 mm tube experiments. Table 2 shows the experimental uncertainties of direct measurements. The uncertainty of local fuel bulk temperature is 0.85 K in terms of measured enthalpy variations. The uncertainty of inner wall temperature is 1.05 K in all experimental conditions because temperature difference between inner and outer wall is limited within 2 K. Furthermore, the temperature difference between inner wall and fuel bulk is higher than 30 K and the uncertainty could be calculated.

$$\left|\frac{\delta(\Delta T)}{\Delta T}\right| = \frac{\sqrt{|\delta T_{wx,in}|^2 + |\delta T_{bx}|^2}}{30} = 4.5\% \tag{8}$$

As the total heat flux and heat loss are two independent variables, the following uncertainty could be obtained based on error propagation formula:

$$\left|\frac{\Delta q_x}{q_x}\right| = \sqrt{\left(\frac{q_x + q_{loss}}{q_x}\right)^2\varepsilon^2(q_{0,x}) + \left(\frac{q_{loss,x}}{q_x}\right)^2\varepsilon^2(q_{loss,x})} \tag{9}$$

In which the uncertainty of total heat flux:

$$\left|\frac{\Delta q_{0,x}}{q_{0,x}}\right| = \sqrt{4\varepsilon^2(I) + \left(\frac{2d_{out}^2}{d_{out}^2 - d_{in}^2}\right)^2\varepsilon^2(d_{out}) + \left(\frac{2d_{in}^2}{d_{out}^2 - d_{in}^2}\right)^2\varepsilon^2(d_{in}) + \varepsilon^2(d_{out})} = 1.37\% \tag{10}$$

Table 2
Experimental uncertainties of direct measurements.

Measured parameters	Instruments	Precisions
Outer wall temperature (K)	K type thermocouple	±0.5 K
Fuel temperature (K)	K type armored thermocouple	±0.5 K
Inner diameter (mm)	Scanning Electron Microscope	±0.0005
Mass flow rate	Coriolis force mass flow-meter	±0.15%
Voltage	Voltmeter with export	±0.2%
Current	Ampere meter with export	±0.2%

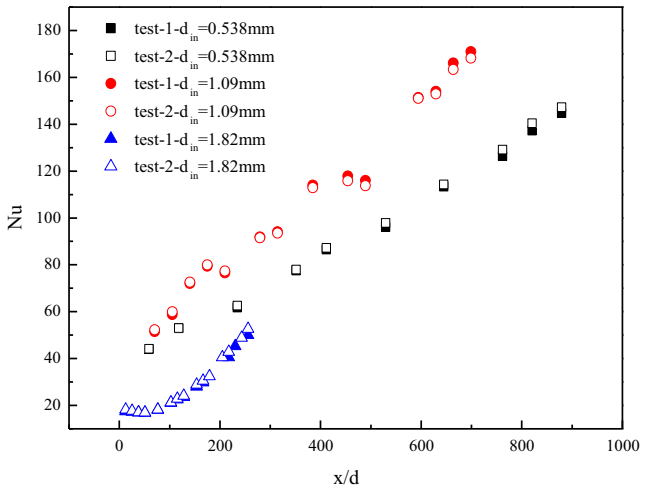

Fig. 4. Repeatability verification of experimental system under identical condition.

And the uncertainty of heat loss:

$$\left|\frac{\Delta q_{loss,x}}{q_{loss,x}}\right| = \sqrt{\varepsilon^2(I) + \varepsilon^2(U) + \varepsilon^2(d_{out}) + \varepsilon^2(L) + \varepsilon^2(T_{wx,out})} = 0.85\% \tag{11}$$

When the ratio between heat loss and effective heat flux is smaller than 5%, the value of Eq. (9) is 1.43%. Above all, the uncertainty of local HTC is obtained.

$$\left|\frac{\Delta h_x}{h_x}\right| = \sqrt{\varepsilon^2(q_x) + \varepsilon^2(\Delta T)} = \sqrt{(1.43\%)^2 + (4.5\%)^2} = 4.73\% \tag{12}$$

The thermal conductivity uncertainty of hydrocarbon fuel is within 3% according to the previous measurement results and the uncertainty of inner diameter is 0.46%. Hence, the maximum uncertainty for Nusselt number could be defined as follows:

$$\left|\frac{\Delta Nu_x}{Nu_x}\right| = \sqrt{\varepsilon^2(h_x) + \varepsilon^2(\lambda) + \varepsilon^2(d_{in})} = \sqrt{(4.73\%)^2 + (3.0\%)^2 + (0.46\%)^2} = 5.62\% \tag{13}$$

Uncertainty analysis for 1.82 mm and 0.538 mm experimental tubes have the same procedure with 1.09 mm tube. Local HTC and Nusselt number uncertainties for 1.82 mm tube are 4.57% and 5.47%, respectively. Also for 0.538 mm tube, the values are 7.11% and 7.77%, respectively.

3. Results and discussion

3.1. Repeatability verification

There will be coking reaction attached to the tube inner wall in the process of heating the hydrocarbon fuel, and then its convective heat transfer characteristics could be influenced. Therefore, the same conditions of verification experiments will be done before and after each experiment, to ensure that the experimental data is true and reliable.

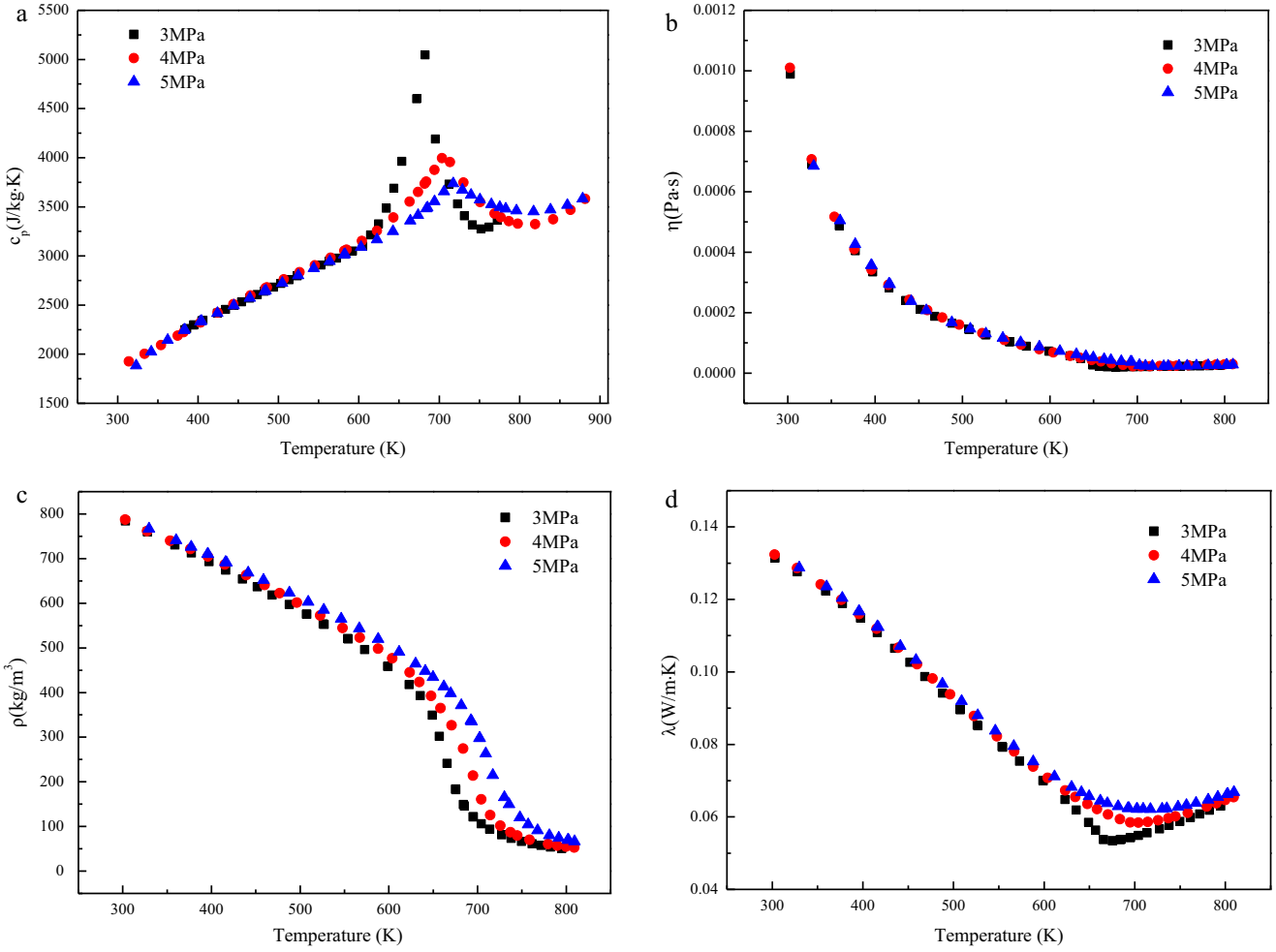

Fig. 5. Thermal properties variations with temperature at 3–5 MPa (a: isobaric specific heat capacity, b: viscosity, c: density, d: thermal conductivity).

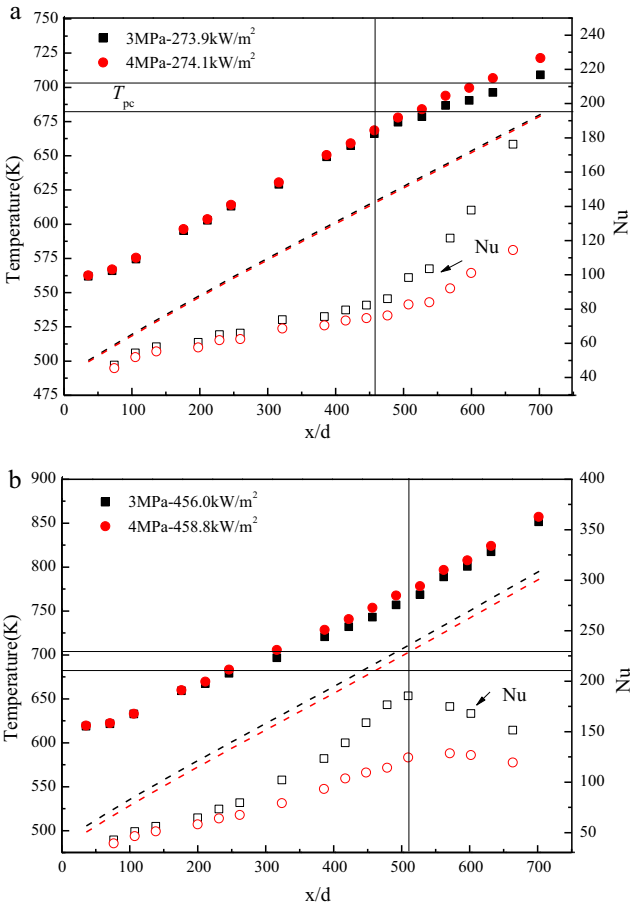

Fig. 6. Temperature and *Nu* number variations under different system pressures.

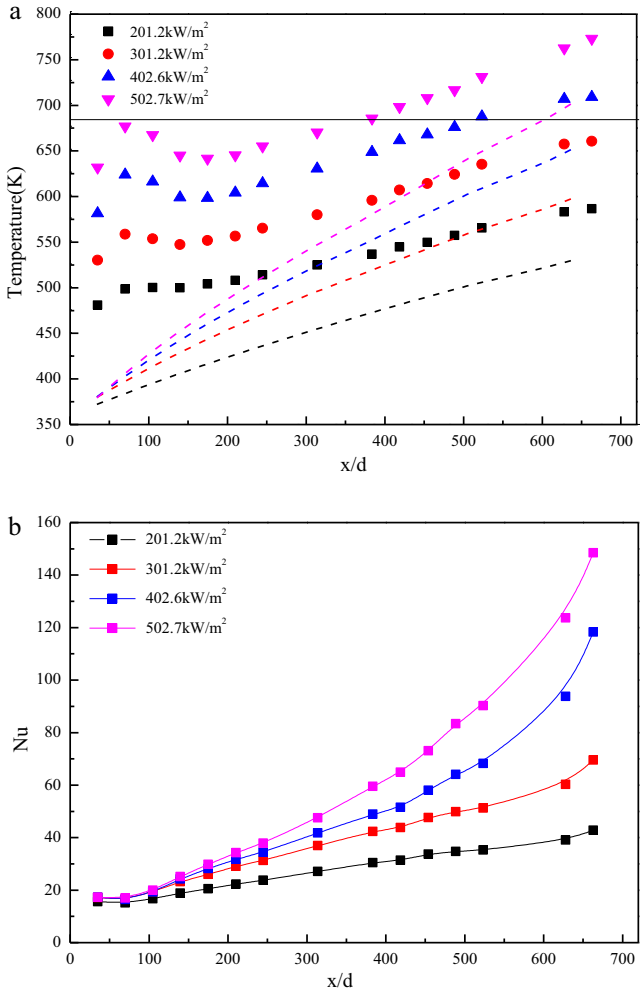

Fig. 7. Temperature and *Nu* number variations under different heat fluxes (inlet Reynolds number is 2800).

Fig. 4 shows three groups of identical experiments in different tubes and it is clearly that two curves of Nusselt number for same conditions are substantially coincident along with dimensionless positions. The maximum deviation of the Nusselt number for 1.82 mm tube is 5.58% and the average deviation is 2.39%. For 1.09 mm tube, the maximum and average deviations are 2.86% and 0.94%, respectively. Also, the two values are 8.5% and 5.69% for 0.538 mm tube. Therefore, all the experiments and its data are verified and repeatable.

3.2. Physical factors effect on heat transfer

3.2.1. Effect of system pressure

System pressure has significant influences on thermal properties of hydrocarbon fuel at supercritical pressures. Isobaric specific heat capacity [38], thermal conductivity [39], viscosity [40] and density [41] variations with bulk temperature at 3 MPa, 4 MPa and 5 MPa pressures are given in Fig. 5. It can be seen from the figure that the heat capacity increases by 1.215 times from $0.85T_{pc}$ to T_{pc} at 3 MPa pressure. However, the increase times for 4 MPa and 5 MPa pressures are 1.271 and 1.203, respectively. The thermal conductivity λ decreases first and then increases with the temperature increasing, and the minimum value appears at the pseudo-critical temperature point corresponding to different pressures. The dynamic viscosity η decreases monotonously with the increase of temperature. The density ρ decreases with increasing temperature and significantly decreases at the pseudo-critical temperature region.

Fig. 6 shows wall temperature, bulk temperature and Nusselt number variations with dimensionless position at two different heat fluxes. For 274 kW/m^2 condition, the fluid average temperature in the test tube is almost the same along the whole tube length. The inner wall temperature is nearly the same in the first half of the tube (dimensionless position x/d < 457), and the second half (dimensionless position x/d > 457) emerges difference as displayed in Fig. 6a. Corresponding to the Nusselt number variation, it gradually increases along the tube length at two pressures. However, the increase velocity of Nusselt number at 3 MPa is larger than that at 4 MPa after the position x/d > 457. It is explained that isobaric specific heat capacity increases by 1.15 times from the temperature 666.1 K to pseudo-critical temperature 682.3 K at 3 MPa pressure. The value at 4 MPa pressure is only 1.04 and heat capacity leads to the key factor on heat transfer enhancement.

The same variation of Nusselt number exists when the heat flux is raised to 457 kW/m^2 as shown in Fig. 6b. While the inner wall temperatures at both 3 MPa and 4 MPa successively reach to the corresponding pseudo-critical temperature, the deviation of Nusselt number becomes more significant at the dimensionless position x/d = 243. Furthermore, the local Nusselt number increases to the peak at the position around x/d = 500, because the fuel bulk temperature is heated to the pseudo-critical temperature. Then the heat transfer deterioration appears due to the sharp increase of heat capacity and obvious increase of thermal conductivity. Over-

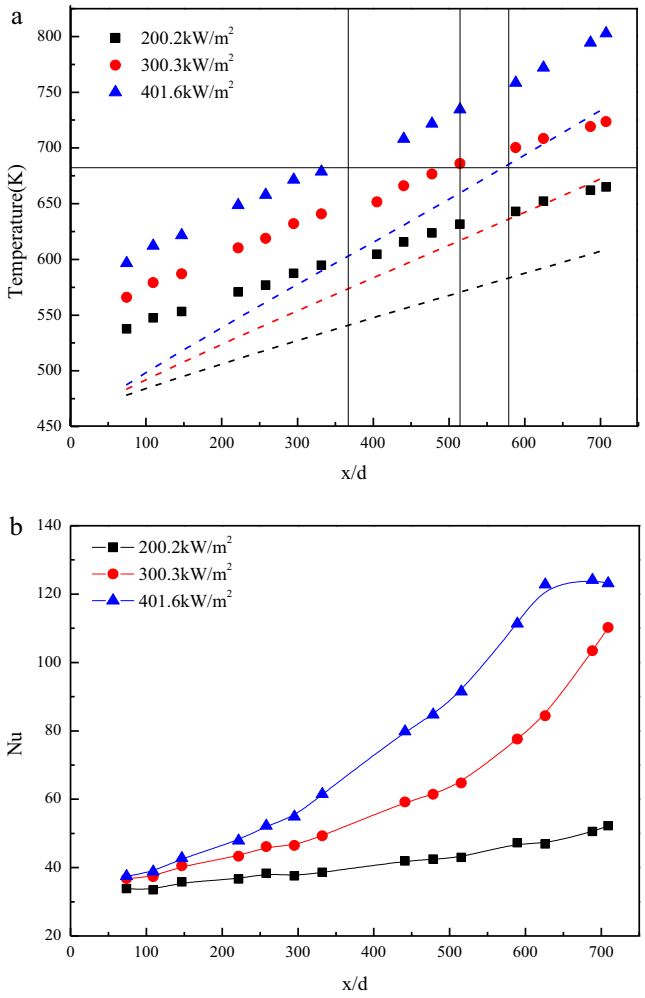

Fig. 8. Temperature and *Nu* number variations under different heat fluxes (inlet Reynolds number is 6600).

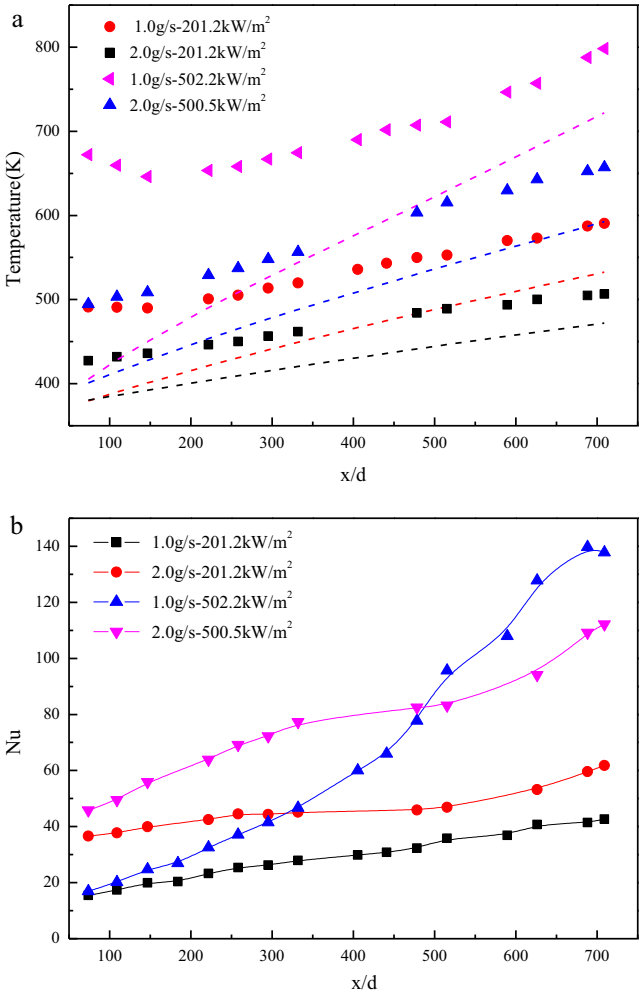

Fig. 9. Temperature and *Nu* number variations under different mass flow rates.

all, thermal properties variations have decisive impact on heat transfer characteristics: decrease of density and thermal conductivity could deteriorate heat transfer, increase of heat capacity and decrease of density could enhance heat transfer.

3.2.2. Effect of heat flux

Fig. 7 shows inner wall temperature, fuel bulk temperature and Nusselt number variations at different heat fluxes in upward flow. The system pressure is fixed at 3 MPa and inlet Reynolds number is about 2800. It can be seen from the figure that the inner wall temperature has the process of first rise and then decline at the inlet region. All the turning points are about at the dimensionless position of x/d = 60. This phenomenon has been observed and explained as 'entrance effect' in previous researches [29,30,42] about supercritical fluid heat transfer. Even though the adiabatic section was set for the fully development of flow boundary layer, the thermal boundary layer would still have a development process. Also, the bulk temperature and isobaric specific heat capacity is relatively low at the initial region, which leads to the weak heat transfer between the wall and fluid. The entrance effect phenomenon becomes more obvious with the increasing of heating heat flux until the thermal boundary layer fully developed at the position of x/d = 140. It is concluded in Fig. 7b that heat transfer capability of the fluid is enhanced due to the temperature influence on thermal properties with the heat flux increasing, and the local Nusselt number gradually increases.

When the inlet Reynolds number is set at high value of 6600, the entrance effect phenomenon at the initial region has disappeared and inner wall temperature monotonically rises along the experimental tube as shown in Fig. 8. It indicates that the inner wall temperature first arrives at the pseudo-critical temperature (P = 3 MPa, T_{pc} = 682.3 K) in the middle of the experimental tube at the heat flux of 401.6 kW/m^2. Then the fuel bulk temperature linearly increases to 682.3 K at the position of x/d = 580. The temperature variation corresponds to linear rise and then exponential increase of the local Nusselt number given in Fig. 8b. For the low heat flux conditions of 200.2 kW/m^2, the steady linear increase of heat transfer capacity is observed due to the relatively low inner wall and bulk temperature under 682.3 K along the whole tube. At the dimensionless position x/d = 650–700, the Nusselt number smoothly increase and tends to be gentle. It is due to the outlet effect that axial heat conduction to isothermal tube part reduces the effective heat flux on flowing aviation kerosene. The effect decreases the convective heat transfer coefficient at the end of experimental tube.

3.2.3. Effect of mass flow rate

The inner wall and fuel bulk temperature variations at two different mass flow rate conditions are shown in Fig. 9a. Mass flow rates are set as 1.0 g/s and 2.0 g/s, and two heat fluxes are 200 kW/m^2 and 500 kW/m^2. The local Reynolds number in the tube varies from 2800 to 9907 when the mass flow rate is 1.0 g/s, while the values are from 5600 to 12,924 at the condition of

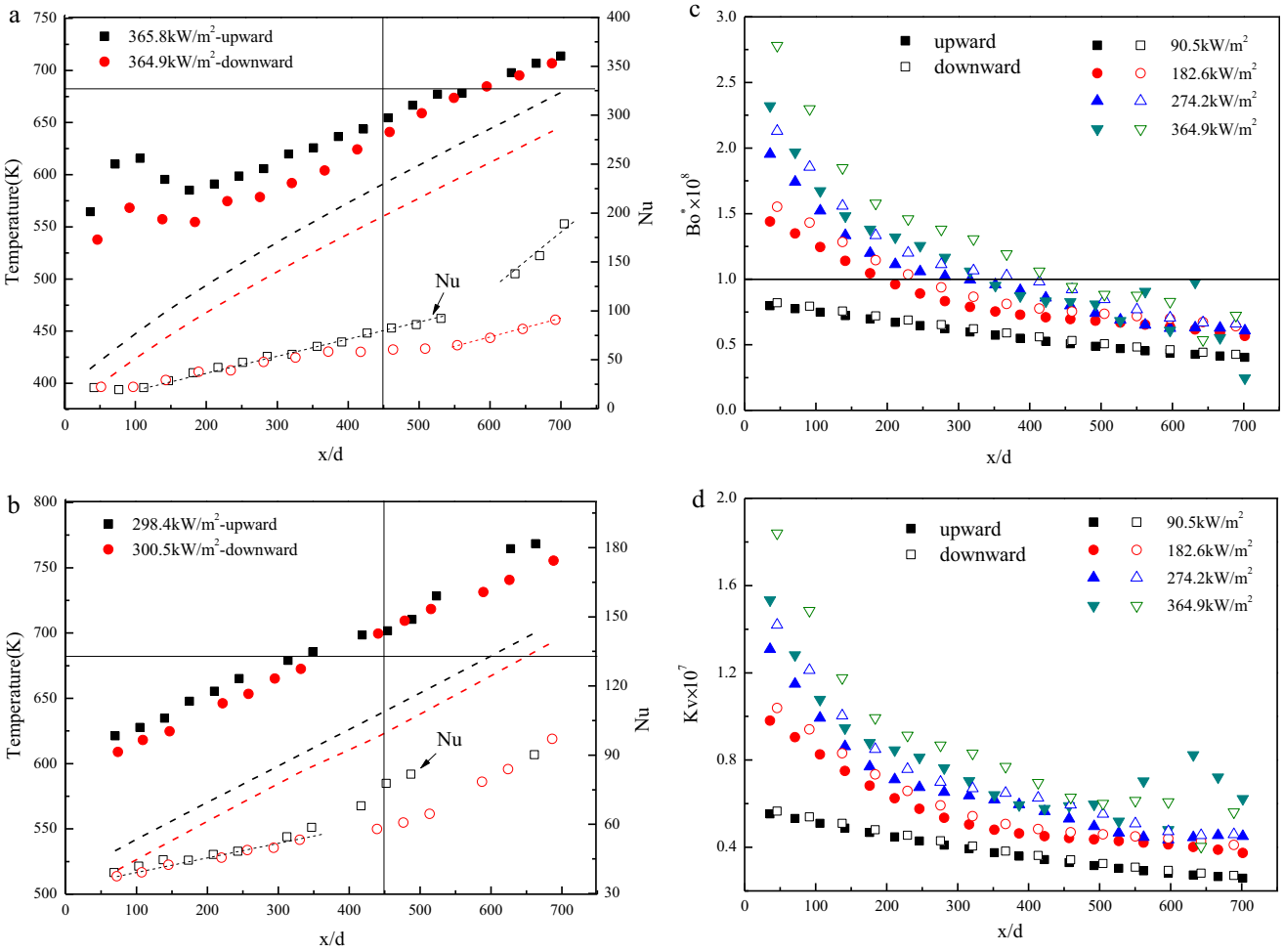

Fig. 10. Temperature, *Nu*, *Bo** and *Kv* number variations under different flow directions.

2.0 g/s. It is clear in figure that the inner wall temperatures almost linearly increase along with the tube at two heat fluxes. However, the inlet inner wall temperature first decreases and then increases because the boundary layer is easy to be influenced at low turbulent kinetic energy conditions. At the condition of 500 kW/m^2, the inner wall temperature achieves to the pseudo-critical temperature at the dimensionless position x/d = 408. For other conditions, all inner wall and fuel bulk temperatures are under 682.3 K. Starting from this point, sharp variation of thermal properties could significantly influence the heat transfer distribution.

Fig. 9b displays local Nusselt number variations at different mass flow rates and heat fluxes. The larger mass flow rate leads to the higher Reynolds numbers distribution, and then induces the better heat transfer capacity. It is obvious that all Nusselt numbers for 2.0 g/s condition have larger value than that for 1.0 g/s at the same heat flux. In addition, the Nusselt number increase linearly along the tube at 1.0 g/s condition and no obvious change is observed when heat flux is 200 kW/m^2. Three periods of heat transfer could be distinguished along the tube: initial region, normal heat transfer and enhanced heat transfer. For 500 kW/m^2 high heat flux condition, the Nusselt number of 1.0 g/s increases to the larger number than that of 2.0 g/s condition. The intersection point is at about x/d = 408 corresponding to the position where inner wall temperature is beyond pseudo-critical temperature as shown in Fig. 9a. It is explained that huge changes of thermal properties could lead to the key factor to enhance the heat transfer.

3.2.4. Effect of flow direction

The biggest difference between upward and downward flow is the effect of buoyancy on heat transfer. The direction of inertial force is different while the direction of buoyancy is always upward, which results in various fluid heat transfer characteristics in different flow directions. Fig. 10a shows temperature and Nusselt number variations along the tube position in both upward and downward flows when the inlet Reynolds number is fixed at 3200. There is a peak in the front wall temperature of the experimental section, and then the wall temperature tends to rise gently with the increase of Reynolds numbers. The entrance effect is obvious in both upward and downward flows that thermal boundary layer develops and thickness increase induces the heat transfer deterioration at the initial region. The buoyancy decreases the shear stress to make flow laminarization, and then heat transfer recovers to the normal with flow development. According to Nusselt number variations, buoyancy effect has nearly same influences on heat transfer when the dimensionless position x/d < 366. The Nusselt number keeps increasing linearly to the value of 65 and the trend remains coincident. At the x/d position between 366 and 600, flow direction starts to influence the heat transfer that Nusselt number remains steady in downward flow because buoyancy restrains the increasing of turbulent kinetic energy. When the inner wall temperature achieves to the pseudo-critical temperature in both flows at about x/d = 600, significant heat transfer enhancement emerges due to sharp variation of thermal properties. Fig. 10b gives the same variations of inner wall temperature

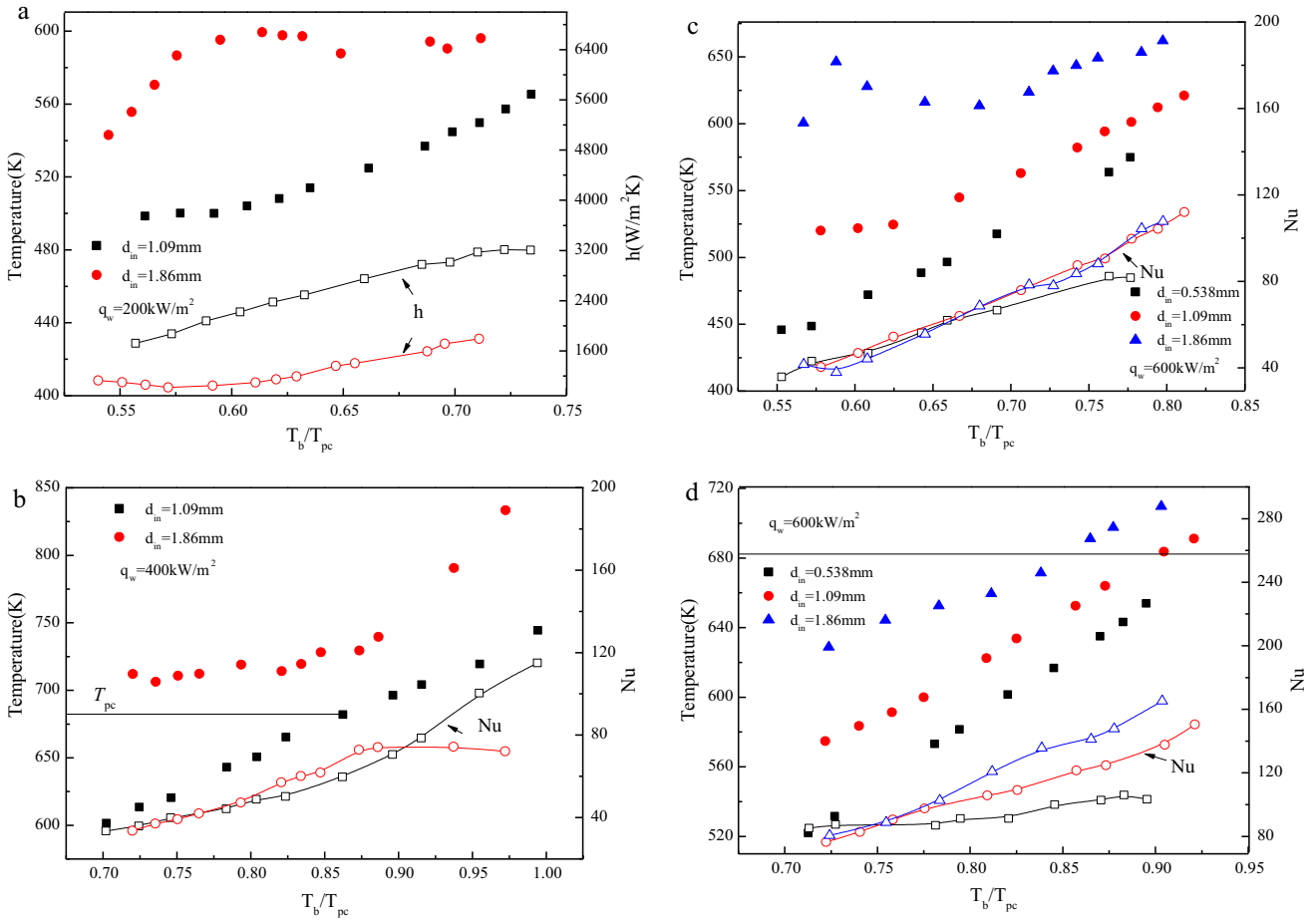

Fig. 11. Effects of inner diameter on heat transfer under various heat fluxes.

and Nusselt number exists at the condition that the inlet Reynolds number is 9550.

Jackson et al. [7,43] analyzed the shear stress variation law along the boundary layer and put forward that 10% reduction of shear stress and heat transfer by taking into account the buoyancy is defined as the demarcation line. Furthermore, one parameter Bo^* was promoted to characterize buoyancy influences on heat transfer in the following equation:

$$Bo^* = \frac{Gr^*}{Re^{3.425}Pr^{0.8}} \tag{14}$$

In which $Gr^* = \frac{\beta g d^4 q_w}{\lambda \nu^2}$ is Grasholf number. The heat transfer is deteriorated when the Bo^* number is between 6×10^{-7} and 1.2×10^{-6} for upward flow. However, heat transfer enhancement phenomena are obviously observed when the Bo^* value is larger than 6×10^{-7}. On the other hand, McEligot et al. [44] proposed thermal acceleration factor Kv to evaluate its effect on heat transfer ability.

$$K\nu = \frac{\nu_b}{u_b^2}\frac{du_b}{dx} = \frac{4q_w\beta}{\rho u_b c_p Re} \tag{15}$$

Fig. 10c shows Bo^* number variation under different fluxes at low and high inlet Reynolds numbers. It is indicated that Bo^* number for most of experimental conditions is far less than 2×10^{-7} obtained in Jiang et al. [45,46] research about n-decane. The reason is that the experimental fluid hydrocarbon fuel is mixture, and not similar to pure fluid n-decane. Moreover, the potential chemical reaction during the high temperature and the smaller inner diameter could make some errors calculating the Bo^* number. Besides, the maximum local Kv displayed in Fig. 10d under various heat fluxes is also far less than the criteria 6×10^{-7} and thermal acceleration could be neglected in aviation kerosene RP-3 experiments in 1.09 mm tube. As talked above, heat transfer is enhanced in the upward flow due to the heat capacity huge increase at the pseudo-critical region. This phenomenon is apparently similar to heat transfer characteristics of laminar mixed convection in miniature vertical tubes. The buoyancy effect is still significant when the Reynolds number gets to the 10^5 level and the phenomenon are similar with Liao and Zhao [47] research. Comparing among all inner wall temperature and Nusselt number data, $Bo^* > 1.0 \times 10^{-8}$ could be summarized as the guideline to evaluate significant influence of buoyancy on heat transfer in 1.09 mm tube.

3.2.5. Effect of tube inner diameter

The Reynolds number is defined in the following equation:

$$Re = \frac{\rho u d}{\eta} = \frac{4\dot{m}}{\eta \pi d_{in}} \tag{16}$$

As long as mass flow rate of the experimental tube is controlled, the entrance of fluid flow status would be determined at the given system pressure and heat flux. Thus, the value of $\dot{m}/d_{in}$ is monitored to the constant to analyze the inner diameter effect on heat transfer. Fig. 11a shows the inner wall temperature and heat transfer coefficient variations along with dimensionless bulk temperature T_b/T_{pc} at the condition of 2800 inlet Reynolds number and 200 kW/m^2 heat flux. It indicates that inner wall temperature in

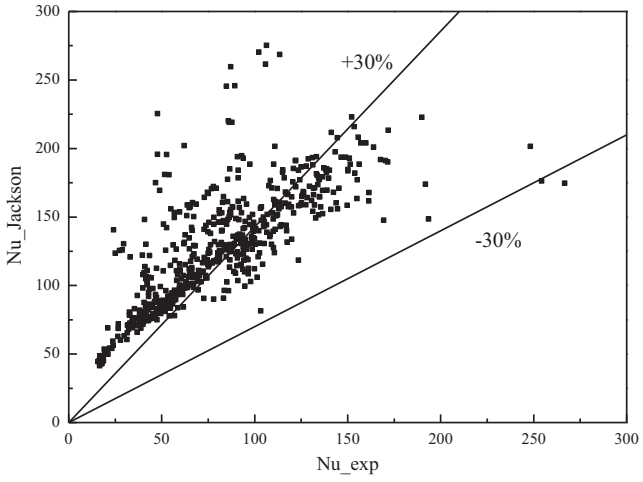

Fig. 12. Comparison between experimental data and calculated values by Jackson formula.

1.82 mm tube is overall larger than that in 1.09 mm tube. Local heat transfer coefficient in 1.09 mm tube is 1.62 times larger than that in 1.82 m tube at the inlet region. Also, buoyancy effect in upward flow in 1.82 mm tube has deteriorated the heat transfer when the inlet Reynolds number is set at 6700 as given in Fig. 11b, which is different from 1.09 mm tube. The Nusselt number variation presents that the diameter effect becomes the key factor after the dimensionless temperature $T_b/T_{pc} > 0.8$.

It is shown in Fig. 11c that inner wall temperature approximately increases linearly under the pseudo-critical temperature when the value of $\dot{m}/d_{in}$ is 1.9. At the contrast temperature between 0.55 and 0.80, Nusselt number in tubes of three different inner diameters shows good agreement. It is explained that thermal properties variations has little effect on heat transfer in different tubes. However, when the inlet Reynolds number increases to 13,200 and contrast temperature varies from 0.70 to 0.95, the inner diameter effect starts to be significant. Fig. 11d displays that the inner wall temperature of 1.82 mm tube first arrives at the pseudo-critical temperature and 0.538 mm tube is the last one. During this period, local heat transfer coefficient of 1.82 mm:1.09 mm:0.538 mm is from 3.72:1.62:1 at the inlet region to 2.19:1.42:1 at the outlet region. At high heat flux conditions, the consistency of Nusselt number variation would be undermined when the contrast temperature is lower than 0.80. Inner diameter and thermal properties combined effects make the larger heat transfer capacity in 0.538 mm tube compared with other two tubes.

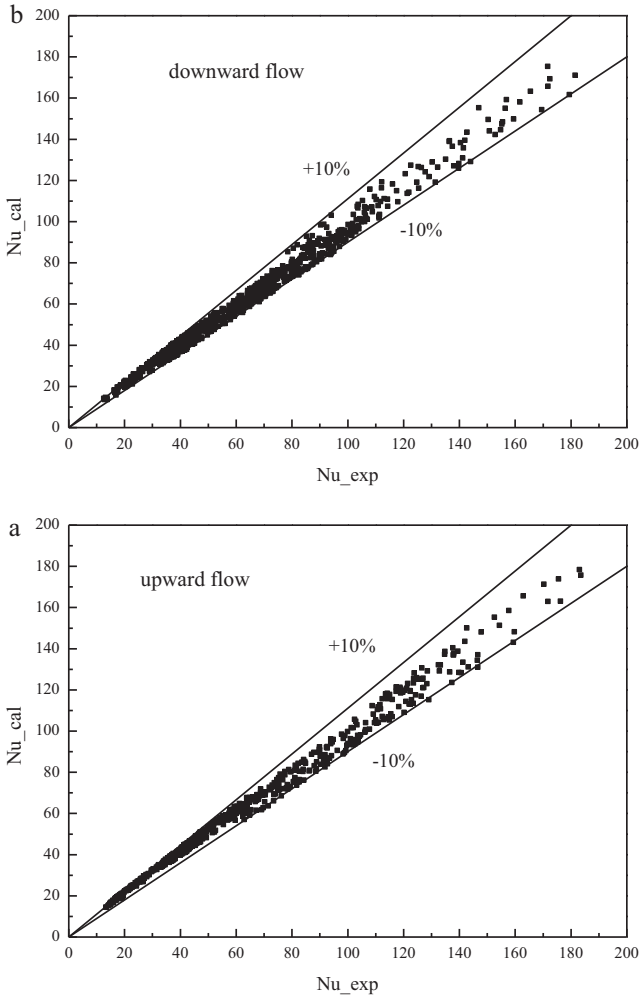

Fig. 13. Comparison between experimental data and new empirical correlation values.

3.3. Heat transfer correlations

Jackson et al. [7] established the semi-empirical formula considering buoyancy influence through theoretical analysis as follows:

$$\frac{Nu}{Nu_f} = \left[\left|1 \pm \frac{8\times 10^4 Gr^*}{Re^{3.425}Pr^{0.8}}\left(\frac{Nu}{Nu_f}\right)^{-2}\right|\right]^{0.46} \tag{17}$$

In the formula, "+" and "−" represent downward and upward flows, respectively. Also, the forced convection correlation is provided in the following equation.

$$Nu_f = 0.0113 Re^{0.862} Pr_f^{0.4} \tag{18}$$

Fig. 12 shows that most of calculated data by Jackson correlation are out of ±30% error band. It is demonstrated that empirical correlation, obtained from experiments with pure substances such as water and carbon dioxide, could produce large errors and is not suitable for hydrocarbon fuels with multiple components and chemical reactions. Thus, all the experimental data in 1.09 mm tube are summarized and two implicit empirical correlations with buoyancy effect are achieved as follows:

For downward flow,

$$\frac{Nu}{Nu_f} = 0.18(10^7 \cdot Bo^*)^{0.1}\left(\frac{\rho_w}{\rho_b}\right)^{0.08}\left(\frac{\eta_w}{\eta_b}\right)^{0.1}\left[1 + 6.8\left(\frac{Nu}{Nu_f}\right)^{1.12}\right] \tag{19}$$

For upward flow,

$$\frac{Nu}{Nu_f} = 0.178(10^7 \cdot Bo^*)^{0.1}\left(\frac{\rho_w}{\rho_b}\right)^{0.11}\left(\frac{\eta_w}{\eta_b}\right)^{0.12}\left[1 + 7.12\left(\frac{Nu}{Nu_f}\right)^{1.09}\right] \tag{20}$$

The relative deviations between experimental values of convective heat transfer and results of the above empirical formula are displayed in Fig. 13. It can be seen that 94.1% of 887 data point for downward flow and 94.7% of upward flow data are within the ±10% error band. Thus, the above two formulas could be used to predict the convective heat transfer of hydrocarbon fuel RP-3 flowing in micro-tubes at supercritical pressures.

4. Conclusion

The convective heat transfer characteristics of aviation kerosene RP-3 at supercritical pressures in vertical micro-tubes with inner diameters of 0.538 mm, 1.09 mm and 1.82 mm under heating conditions were studied. The following results are obtained:

(1) System pressure and heat flux affect the heat transfer in essence by influencing the fuel thermo-physical properties. Normal, deterioration and enhancement of heat transfer generally occurs in turn with dimensionless position.
(2) Nusselt number variations show good agreement when $T_b/T_{pc} < 0.8$ in different tubes and small inner diameter has better heat transfer at large contrast temperatures.
(3) Buoyancy effect is still significant at the Reynolds number higher than 10^5 in 1.09 mm tube and $Bo^* = 1.0 \times 10^{-8}$ could be the critical point to evaluate buoyancy influence.
(4) Two empirical correlations of Nusselt number to summarize downward and upward flow heat transfer in 1.09 mm tube are proposed with good prediction.

References

[1] P. Bourke, D. Pulling, L. Gill, W. Denton, Forced convective heat transfer to turbulent CO_2 in the supercritical region, Int. J. Heat Mass Transfer 13 (8) (1970) 1339–1348.
[2] K. Yamagata, K. Nishikawa, S. Hasegawa, T. Fujii, S. Yoshida, Forced convective heat transfer to supercritical water flowing in tubes, Int. J. Heat Mass Transfer 15 (12) (1972) 2575–2593.
[3] E. Krasnoshchekov, V. Protopopov, Experimental study of heat exchange in carbon dioxide in the supercritical range at high temperature drops (heat transfer in turbulent carbon dioxide pipeflow at supercritical region), High Temp. 4 (1966) 375–382.
[4] W. Hall, Heat transfer near the critical point, Adv. Heat Transfer 7 (1971) 1–86.
[5] W.B. Hall, J. Jackson, Laminarization of a turbulent pipe flow by buoyancy forces, in: Mechanical Engineering, ASME-345 E 47th St., NewYork, NY 10017, 1969, pp. 66.
[6] J. Jackson, W. Hall, Forced convection heat transfer to fluids at supercritical pressure, Turbul. Forced Convect. Channels Bundles 2 (1979) 563–611.
[7] J. Jackson, M. Cotton, B. Axcell, Studies of mixed convection in vertical tubes, Int. J. Heat Fluid Flow 10 (1) (1989) 2–15.
[8] J.K. Kim, H.K. Jeon, J.S. Lee, Wall temperature measurement and heat transfer correlation of turbulent supercritical carbon dioxide flow in vertical circular/non-circular tubes, Nucl. Eng. Des. 237 (15) (2007) 1795–1802.
[9] H. Kim, H.Y. Kim, J.H. Song, Y.Y. Bae, Heat transfer to supercritical pressure carbon dioxide flowing upward through tubes and a narrow annulus passage, Prog. Nucl. Energy 50 (2–6) (2008) 518–525.
[10] Y.-Y. Bae, H.-Y. Kim, Convective heat transfer to CO_2 at a supercritical pressure flowing vertically upward in tubes and an annular channel, Exp. Therm. Fluid Sci. 33 (2) (2009) 329–339.
[11] P.-X. Jiang, Y. Zhang, Y.-J. Xu, R.-F. Shi, Experimental and numerical investigation of convection heat transfer of CO_2 at supercritical pressures in a vertical tube at low Reynolds numbers, Int. J. Therm. Sci. 47 (8) (2008) 998–1011.
[12] P.-X. Jiang, Y.-J. Xu, J. Lv, R.-F. Shi, S. He, J. Jackson, Experimental investigation of convection heat transfer of CO_2 at super-critical pressures in vertical mini-tubes and in porous media, Appl. Therm. Eng. 24 (8) (2004) 1255–1270.
[13] P.-X. Jiang, R.-F. Shi, Y.-J. Xu, S. He, J. Jackson, Experimental investigation of flow resistance and convection heat transfer of CO_2 at supercritical pressures in a vertical porous tube, J. Supercrit. Fluid 38 (3) (2006) 339–346.
[14] P.-X. Jiang, B. Liu, C.-R. Zhao, F. Luo, Convection heat transfer of supercritical pressure carbon dioxide in a vertical micro tube from transition to turbulent flow regime, Int. J. Heat Mass Transfer 56 (1) (2013) 741–749.
[15] T. Yamashita, H. Mori, S. Yoshida, M. Ohno, Heat transfer and pressure drop of a supercritical pressure fluid flowing in a tube of small diameter, Mem. Facul. Eng. 63 (4) (2003) 227–244.
[16] D.R. Sobel, L.J. Spadaccini, Hydrocarbon fuel cooling technologies for advanced propulsion, J. Eng. Gas Turb. Power 119 (2) (1997) 344–351.
[17] G. Bruening, W. Chang, Cooled Cooling Air Systems for Turbine Thermal Management, ASME Paper, 99-GT, 1999, p. 14.
[18] B. Hitch, M. Karpuk, Experimental investigation of heat transfer and flow instabilities in supercritical fuels, AIAA Paper 3043 (1997).
[19] B. Hitch, M. Karpuk, Enhancement of heat transfer and elimination of flow oscillations in supercritical fuels, AIAA 3759 (1998).
[20] W. Hines, Pressure oscillations associated with heat transfer to hydrocarbon fluids at supercritical pressures and temperatures, ARS J. 32 (3) (1962) 361–366.
[21] X. Fan, F. Zhong, G. Yu, J. Li, C. Sung, Catalytic cracking and heat sink capacity of aviation kerosene under supercritical conditions, J. Propul. Power 25 (6) (2009) 1226–1232.
[22] W. Li, D. Huang, G.-Q. Xu, Z. Tao, Z. Wu, H.-T. Zhu, Heat transfer to aviation kerosene flowing upward in smooth tubes at supercritical pressures, Int. J. Heat Mass Transfer 85 (2015) 1084–1094.
[23] L. Zhang, R.L. Zhang, S.D. Xiao, J. Jiang, J.L. Le, Experimental investigation on heat transfer correlations of n-decane under supercritical pressure, Int. J. Heat Mass Transfer 64 (2013) 393–400.
[24] K. Zhu, G.-Q. Xu, Z. Tao, H.-W. Deng, Z.-H. Ran, C.-B. Zhang, Flow frictional resistance characteristics of kerosene RP-3 in horizontal circular tube at supercritical pressure, Exp. Therm. Fluid Sci. 44 (2013) 245–252.
[25] Z. Liu, H. Pan, S. Feng, Q. Bi, Dynamic behaviors of coking process during pyrolysis of China aviation kerosene RP-3, Appl. Therm. Eng. 91 (2015) 408–416.
[26] K. Xu, H. Meng, Numerical study of fluid flows and heat transfer of aviation kerosene with consideration of fuel pyrolysis and surface coking at supercritical pressures, Int. J. Heat Mass Transfer 95 (2016) 806–814.
[27] D. Huang, X.-Y. Wu, Z. Wu, W. Li, H.-T. Zhu, B. Sunden, Experimental study on heat transfer of nanofluids in a vertical tube at supercritical pressures, Int. Commun. Heat Mass Transfer 63 (2015) 54–61.
[28] K.A. Misurati, Y. Quan, W. Gong, G. Xu, Y. Yan, Contrastive study of flow and heat transfer characteristics in a helically coiled tube under uniform heating and one-side heating, Appl. Therm. Eng. 114 (2017) 77–84.
[29] C. Zhang, G. Xu, L. Gao, Z. Tao, H. Deng, K. Zhu, Experimental investigation on heat transfer of a specific fuel (RP-3) flows through downward tubes at supercritical pressure, J. Supercrit. Fluid 72 (2012) 90–99.
[30] C. Zhang, G. Xu, J. Sun, Z. Jin, Modified k–ε model for RP-3 kerosene in a horizontal circular tube at supercritical pressure, Appl. Therm. Eng. 102 (2016) 1403–1411.
[31] S. Yildiz, D. Groeneveld, Diameter effect on supercritical heat transfer, Int. Commun. Heat Mass Transfer 54 (2014) 27–32.
[32] J. Ackerman, Pseudoboiling heat transfer to supercritical pressure water in smooth and ribbed tubes, J. Heat Transfer – Trans. ASME 92 (3) (1970) 490–497.
[33] J. Song, H. Kim, H. Kim, Y. Bae, Heat transfer characteristics of a supercritical fluid flow in a vertical pipe, J. Supercrit. Fluid 44 (2) (2008) 164–171.
[34] J. Wang, H. Li, S. Yu, T. Chen, Comparison of the heat transfer characteristics of supercritical pressure water to that of subcritical pressure water in vertically-upward tubes, Int. J. Multiphase Flow 37 (7) (2011) 769–776.
[35] M. Watts, C. Chou, Mixed convection heat transfer to supercritical pressure water, in: Proceedings of the 7th International Heat Transfer Conference, 1982, pp. 495–500.
[36] A. Tanase, S. Cheng, D. Groeneveld, J. Shan, Diameter effect on critical heat flux, Nucl. Eng. Des. 239 (2) (2009) 289–294.
[37] C. Zhang, H. Deng, G. Xu, W. Huang, K. Zhu, Enthalpy measurement and heat transfer investigation of RP-3 kerosene at supercritical pressure, J. Aerosp. Power 25 (2) (2010) 331–335.
[38] H. Deng, K. Zhu, G. Xu, Z. Tao, C. Zhang, G. Liu, Isobaric specific heat capacity measurement for kerosene RP-3 in the near-critical and supercritical regions, J. Chem. Eng. Data 57 (2) (2011) 263–268.
[39] G. Xu, Z. Jia, J. Wen, H. Deng, Y. Fu, Thermal-conductivity measurements of aviation kerosene RP-3 from (285 to 513) K at sub-and supercritical pressures, Int. J. Thermophys. 36 (4) (2015) 620–632.
[40] H. Deng, C. Zhang, G. Xu, B. Zhang, Z. Tao, K. Zhu, Viscosity measurements of endothermic hydrocarbon fuel from (298 to 788) K under supercritical pressure conditions, J. Chem. Eng. Data 57 (2) (2012) 358–365.
[41] H. Deng, C. Zhang, G. Xu, Z. Tao, B. Zhang, G. Liu, Density measurements of endothermic hydrocarbon fuel at sub-and supercritical conditions, J. Chem. Eng. Data 56 (6) (2011) 2980–2986.
[42] X. Li, X. Huai, J. Cai, F. Zhong, X. Fan, Z. Guo, Convective heat transfer characteristics of China RP-3 aviation kerosene at supercritical pressure, Appl. Therm. Eng. 31 (14–15) (2011) 2360–2366.
[43] J.D. Jackson, Fluid flow and convective heat transfer to fluids at supercritical pressure, Nucl. Eng. Des. 264 (2013) 24–40.
[44] D. McEligot, C. Coon, H. Perkins, Relaminarization in tubes, Int. J. Heat Mass Transfer 13 (2) (1970) 431–433.
[45] B. Liu, Y. Zhu, J.-J. Yan, Y. Lei, B. Zhang, P.-X. Jiang, Experimental investigation of convection heat transfer of *n*-decane at supercritical pressures in small vertical tubes, Int. J. Heat Mass Transfer 91 (2015) 734–746.
[46] Y. Zhu, B. Liu, P. Jiang, Experimental and numerical investigations on *n*-decane thermal cracking at supercritical pressures in a vertical tube, Energy Fuels 28 (1) (2013) 466–474.
[47] S. Liao, T. Zhao, An experimental investigation of convection heat transfer to supercritical carbon dioxide in miniature tubes, Int. J. Heat Mass Transfer 45 (25) (2002) 5025–5034.